

Viscoelastic Micellar Solutions in Nonionic Fluorinated Surfactant Systems

Durga P. Acharya,[†] Suraj Chandra Sharma,[†] Carlos Rodriguez-Abreu,[‡] and Kenji Aramaki^{*,†}

Graduate School of Environment and Information Sciences, Yokohama National University, 79-7 Tokiwadai, Hodogaya-ku, Yokohama 240-8501, Japan, and Departamento de Química Física, Facultad de Química, Universidad de Santiago de Compostela, E-15782 Santiago de Compostela, Spain

Received: June 19, 2006; In Final Form: July 26, 2006

The formation and rheological behavior of a viscoelastic wormlike micellar solution in an aqueous solution of a nonionic fluorinated surfactant, perfluoroalkyl sulfonamide ethoxylate, of structure $\text{C}_8\text{F}_{17}\text{SO}_2\text{N}(\text{C}_3\text{H}_7)(\text{CH}_2\text{CH}_2\text{O})_{10}\text{H}$ was studied. Temperature-induced viscosity growth is observed even at low-surfactant concentration (~ 1 wt %), and viscosity reaches the maximum at a temperature $T_{\eta\text{-max}}$. Upon successive increases in the temperature, the viscosity decreases, and ultimately a phase separation occurs. Small-angle X-ray scattering (SAXS) measurements confirm the presence of cylindrical aggregates at low temperature, which undergo continuous one-dimensional growth with increasing temperature, and ultimately, an indication of a slight lamellarlike structural pattern is observed, which probably comes from the formation of micellar joints or branching. Such changes in the microstructure result in a decrease in the viscosity and stress-relaxation time, while the network structure is retained; the trends in the evolution of shear modulus (G_0) and relaxation time (τ_R) with temperature are in agreement with this. With increased surfactant concentration, the temperature corresponding to the viscosity maximum ($T_{\eta\text{-max}}$) in the temperature–viscosity curve shifts to lower values, and the viscosity at temperatures below or around $T_{\eta\text{-max}}$ increases sharply. A viscoelastic solution with Maxwellian-type dynamic rheological behavior at low-shear frequency is formed, which is typical of entangled wormlike micelles. Rheological parameters, η_0 and G_0 , show scaling relationships with the surfactant concentrations with exponents slightly greater than the values predicted by the living-polymer model, but the exponent of τ_R is in agreement with the theory. Dynamic light-scattering measurements indicate the presence of fast relaxation modes, associated with micelles, and medium and slow modes, associated with transient networks. The disappearance of the slow mode and the predominance of the medium mode as the temperature increases support the conclusions derived from SAXS and rheometry.

Introduction

Perfluorosurfactants behave in a manner similar to that of their hydrocarbon analogues. Above critical micelle concentration (cmc), they form micelles, threadlike micelles, vesicles, lamellar aggregates, and other various liquid crystalline structures in solution. Similar phase sequences are observed in fluorinated-surfactant and hydrocarbon-surfactant systems when solution conditions are changed, for example, when the surfactant concentration is changed. However, perfluorosurfactants are more hydrophobic and reduce the surface tension of an aqueous solution to an extent which is unattainable with hydrocarbon surfactants. Similarly, they show a much lower cmc than hydrocarbon-chain surfactants of same length.^{1,2} Atomic properties of fluorine (viz., its high electronegativity, its relatively large van der Waals radius, and less conformational freedom (mainly all trans) of the fluorinated chain) produce bulky and stiff chains with their skeletons covered by a dense electro-rich environment. It is easier to pack a fluorocarbon chain closely because the chains are in all-trans states and less entropy is lost. As a result, these surfactants have high chemical and thermal stability and therefore are useful in many practical applications where hydrocarbon surfactants would decompose.

The aggregate structures in fluorinated surfactants can be explained, like hydrocarbon surfactants, in terms of the value of critical packing parameter,³ $CPP = v/a_s l$, where v is the volume hydrophobic part, l is its length, and a_s is the average area of headgroup at the interface. However, the fluorocarbon chains are bulkier than the hydrocarbon chain with the volume of $-\text{CF}_2$ and terminal $-\text{CF}_3$ being 0.041 and 0.084 nm³, respectively, compared with 0.027 and 0.037 nm³, respectively, for hydrocarbon analogues.⁴ Therefore, to form a spherical aggregate ($CPP \leq 1/3$), fluorinated surfactants with very large headgroups are needed to balance the effect of the bulky fluorocarbon chain.⁵ Therefore, cylindrical micelles are often observed at solution conditions where spherical micelles are expected in hydrocarbon-surfactant systems. These cylindrical micelles often undergo enormous one-dimensional growth and form flexible threadlike aggregates called “wormlike micelles”. This type of growth is attributed to effort of the system to reduce the high free-energy cost associated with the formation of hemispherical end caps when the solution properties favor spontaneous curvature of cylinders. The system can reduce the free energy by reducing the number of free ends, that is, by end-to-end fusion of several short cylindrical aggregates to form a long aggregate. When the number density of the wormlike aggregates exceeds a certain threshold value, they entangle each other to form a transient network and exhibit viscoelastic properties.

The formation and properties of viscoelastic wormlike micelles have been studied extensively for hydrocarbon sur-

* To whom correspondence should be addressed. E-mail: aramakik@ynu.ac.jp. Phone/Fax: +81-45-339 4300.

[†] Yokohama National University.

[‡] Universidad de Santiago de Compostela.

factants, mostly in long hydrophobic-chain (C_{16} or longer) cationic surfactants in the presence of excess counterions^{6–12} and, in some cases, even in absence of excess counterions if the counterions are strongly bound at the hydrophilic–hydrophobic interface.^{13–16} Viscoelastic solutions of wormlike micelles have also been reported in cationic or anionic fluorinated-surfactant aqueous systems, even at a relatively short fluorocarbon-chain lengths.^{17–19} The effect of the concentration of the counterions and the surfactant concentration on the rheological behavior and micellar growth is more or less similar in both types of surfactants.¹⁹ There are reports of thermoresponsive viscoelasticity in some hybrid anionic surfactants containing both fluorocarbon and hydrocarbon chains in their molecules.^{20–23}

Only a few reports on the formation of viscoelastic wormlike micellar solutions and the study of their rheological behavior are available in aqueous systems of nonionic hydrocarbon surfactants, such as ethoxylated sterols^{24–26} and sucrose alkanolates.²⁷ In these systems, interfacial curvature of the aggregates can be tuned to induce the sphere–rod transition and one-dimensional micellar growth via the addition of a lipophilic surfactant, such as polyoxyethylene alkyl ether or long-chain monoglyceride. A similar tendency is observed in ionic surfactant solutions as well.^{28–32} An aqueous solution of a surfactant with a cholesteric group as the hydrophobic part formed a viscoelastic solution at elevated temperature.³³ However, not much is known about the formation and rheological behavior of wormlike micelles in nonionic systems. Knowledge about the formation and rheological properties of nonionic systems is important not only to obtain a better understanding of the underlying basic principle of the phenomenon but also for practical applications, such as in cosmetics and toiletry products, because of the absence of charged species and improved mildness to the skin.

In this paper, we present our study on the temperature-induced viscosity growth in a water–surfactant binary system of a nonionic fluorinated surfactant, perfluoroalkyl sulfonamide ethoxylate, at various concentrations. To our knowledge, this is the only nonionic surfactant known so far which forms a viscoelastic solution of wormlike micelles in a surfactant–water binary system,³⁴ but little is known about its rheological behavior. In this study, the microstructural change in the aggregates as a function of temperature and composition is studied by rheometry and dynamic light scattering (DLS). The small-angle X-ray scattering (SAXS) technique has been used to obtain direct evidence of the shape change and the internal structure of the aggregates.

Theoretical Background.

SAXS. Small-angle scattering data can be analyzed by indirect Fourier transformation (IFT) followed by deconvolution.^{35–39} This method allows us to extract information about the shape and internal structure without having a priori assumption on the model of the aggregate. Only an outline of the principle is presented here.

When the system is sufficiently dilute, so that the effect of the interparticle interference scattering, that is, the structure factor, $S(q) \approx 1$, the spatially averaged q -dependent scattering intensity, $I(q)$, is given by

$$I(q) = 4\pi \int_0^\infty p(r) \frac{\sin qr}{qr} dr \quad (1)$$

where $p(r)$ is the pair-distance distribution function (PDDF), involving the information about the size, shape (see Figure 1), and even, internal core–shell structure of particles such as micellar aggregates. The intraparticle scattering contribution is

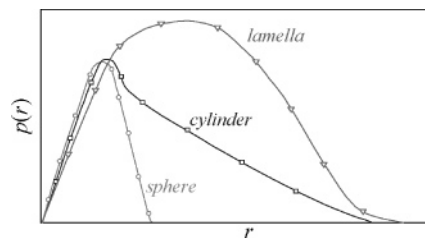


Figure 1. Schematic PDDFs, $p(r)$, for homogeneous particles of three different shapes.

called the form factor, $P(q)$, which theoretically corresponds to the Fourier transform of $p(r)$. The PDDF for a particle of an arbitrary shape with a scattering density difference of $\Delta\rho(r)$ is given by

$$p(r) = r^2 \Delta\tilde{\rho}^2(r) \quad (2)$$

where $\Delta\tilde{\rho}^2(r)$ is the convolution square of $\Delta\rho(r)$ averaged over all directions in space. For a spherical particle, averaging is not necessary because the scattering-density difference or electron-density difference, $\Delta\rho_s(r)$, is only a function of the radial position, and deconvolution of PDDF gives the radius contrast profile. For cylindrical-scattering particles, such as rodlike micelles, the situation is similar to a sphere within a cross-section (i.e., the contrast profile, $\Delta\rho_c(r)$, is a function of the radial position within the cross-section), and the overall PDDF can be obtained from the Fourier transformation of the $I(q)$ curve. The linear region of $p(r)$ at large r in the PDDF pattern of a cylindrical particle (see Figure 1) comes from its axial length. If the cylinder is at least 3 times longer than the cross-sectional diameter, it is possible to obtain the radial profile, $\Delta\rho_c(r)$, which is related to the PDDF for the cross section, $p_c(r)$, by

$$p_c(r) = r^2 \Delta\tilde{\rho}_c^2(r) \quad (3)$$

The cross sectional PDDF, $p_c(r)$, is related to scattered intensity by a particle of length L by the following relation:

$$I(q) = \frac{\pi L I_c(q)}{q} = \frac{2\pi^2 L}{q} \int_0^\infty p_c(r) J_0(qr) dr \quad (4)$$

where $J_0(qr)$ is the zero-order Bessel function and $I_c(q)$ is the cross-sectional scattering function. The indirect Fourier transformation of above equation gives $p_c(r)$, which in turn can be used to obtain $\Delta\rho_c(r)$.

When the contribution of interparticle interference to the scattering becomes significant, the overall $I(q)$ for the systems of monodisperse spherical particles is given by

$$I(q) = nP(q)S(q)$$

In this case, scattering data can be analyzed by the *generalized indirect Fourier transformation* (GIFT) technique^{40,41} which allows us to determine the form factor and the structure factor simultaneously from the scattering data without any assumption for the form factor, whereas we need appropriate assumptions for the interparticle interaction potential and the closure relation for the structure factor. The detailed theoretical description on the method has been reported elsewhere.^{31,33} Note that when particle geometry deviates from an ideal spherical symmetry, the output parameters from $S(q)$ analysis are no longer exact. Nevertheless, the GIFT approach efficiently suppresses the

influence of the interparticle interference scattering in the calculation of $p(r)$ and allows us to deduce a sufficiently reliable $p(r)$ value.

The typical patterns of the PDDFs of homogeneous spherical, cylindrical, and flat particles are shown in Figure 1. For a cylindrical aggregate, the distance in the low- r region, at which $p(r)$ decreases sharply after the maximum, gives a cross-sectional diameter of the aggregates, whereas the value of r at which $p(r)$ becomes zero gives the maximum dimension of the aggregate, D_{\max} (i.e., the length of the cylindrical micelles).

Rheological Behavior of Wormlike Micelles. When the network of wormlike micelles is deformed or the equilibrium conditions are suddenly changed, the relaxation occurs within a definite time, and the equilibrium condition is restored again. For a deformation with a time period shorter than the relaxation time, τ_R , the system exhibits an elastic property characteristic of a solid material with a Hookean constant, G_0 , called the shear modulus. For a slow deformation, however, the network has sufficient time to dissipate the stress, and the viscoelastic system behaves as a viscous fluid with a zero-shear viscosity, η_0 .

The rheological behavior of a viscoelastic material can be investigated by applying a small-amplitude sinusoidal deformation. The behavior can be described by a mechanical model, called the Maxwell model,^{42,43} consisting of an elastic spring with the Hookean constant, G_0 , and a dashpot with the viscosity, η_0 . The variation of storage modulus (G') and loss modulus (G'') with shear frequency, ω , are given by the equations

$$G'(\omega) = \frac{\omega^2 \tau_R^2}{1 + \omega^2 \tau_R^2} G_0 \quad (5)$$

$$G''(\omega) = \frac{\omega \tau_R}{1 + \omega^2 \tau_R^2} G_0 \quad (6)$$

where τ_R is the relaxation time. The parameters G' and G'' are the elastic and viscous components of complex shear modulus, and they are related to the ability of the material to behave as an elastic or viscous material. As evident from the Maxwell equations, in the low-frequency region, $\omega \ll \omega_c$, G' and G'' scale with ω according to $G' \approx \omega^2$ and $G'' \approx \omega$. In the high-frequency region, or more specifically, in the region of $\omega \gg \omega_c$, however, G' attains a plateau value equal to G_0 , whereas G'' shows a monotonic decrease. The shear frequency corresponding to $G' - G''$ crossover, ω_c , is equal to the inverse of τ_R . For wormlike micelles at particular conditions, the magnitude of τ_R is related to the average length of the wormlike micelles, whereas G_0 is related to the number density of the entanglement in the transient network.

Once G_0 and τ_R are available, η_0 can be calculated using following relation:

$$\eta_0 = G_0 \tau_R \quad (7)$$

Alternately, the following relationship allows one to estimate η_0 by extrapolating the complex viscosity values ($|\eta^*|$) to zero shear frequency:

$$|\eta^*| = \frac{(G'^2 + G''^2)^{1/2}}{\omega} = \frac{\eta_0}{\sqrt{1 + \omega^2 \tau_R^2}} \quad (8)$$

The living-polymer model proposed by Cates et al.^{44–46} considers the molecular-weight distribution (MWD) of the wormlike micelle to be in a thermal equilibrium, and such systems are called an equilibrium polymer or “living polymer”,

which is in contrast to the fixed MWD of ordinary polymer solutions. The viscoelastic behavior of the entangled wormlike micelles is described by considering two processes, reptation (i.e., reptilelike motion of the micelle along its own contour) and reversible scission of micelles, taking place at two time scales, namely, reptation time, τ_{rep} , and breaking time, τ_b . The τ_{rep} is the time required for a wormlike micelle of contour length \bar{L} to pass through an hypothetical tube, and the τ_b is the average time necessary for a chain of average length \bar{L} to break into two pieces. It is assumed that when a chain breaks, the two daughter chains become uncorrelated and recombine with the micellar end in random way. For fast scission kinetics ($\tau_b \ll \tau_{\text{rep}}$), a single-exponential stress decay is observed, and the viscoelastic behavior of such systems in the low-frequency region follows the Maxwell model with a single relaxation time, τ_R , given by $(\tau_b \tau_{\text{rep}})^{1/2}$.⁴⁴

Although the Maxwell equations predict a monotonic decrease of G'' in the high-frequency region, the wormlike micelles deviate from this behavior, showing an increase of G'' in the high-frequency region and a deviation from the semicircle, as well as a depression in a Cole–Cole plot of G'' versus G' . This deviation is often associated with the stress relaxation by additional “faster” processes such as Rouse modes of cylindrical micelles, analogous to the polymer chain. The minimum value of G'' in the high-frequency region is related to \bar{L} according to the relation⁴⁵

$$\frac{G''_{\min}}{G_0} \approx \frac{l_e}{\bar{L}} \quad (9)$$

where l_e is the entanglement length, the contour length of the section of wormlike micelles between two entanglement points. For flexible micelles, the correlation length, ξ , which gives the mesh size of the micellar network, is related to l_e according to⁴⁵

$$l_e \approx \xi^{5/3} / l_p^{2/3} \quad (10)$$

The persistence length, l_p , gives an estimate of micellar flexibility. Even though the micelles are flexible, at a small-length scale comparable to l_p , they behave as rigid rods. Also,

$$\xi = \left(\frac{kT}{G_0} \right)^{1/3} \quad (11)$$

The combination of eqs 10 and 11 yields a relation which relates l_e to G_0 .⁴⁵

$$G_0 \approx \frac{kT}{l_e^{9/5} l_p^{6/5}} \quad (12)$$

In the limit $\tau_b \ll \tau_{\text{rep}}$, the living-polymer model predicts the following scaling laws for the viscoelastic parameters:^{46,47}

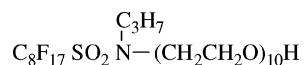
$$G_0 \approx \phi^{2.25} \quad (13)$$

$$\tau_R \approx \phi^{1.25} \quad (14)$$

$$\eta_0 \approx \phi^{3.5} \quad (15)$$

$$\frac{G''_{\min}}{G_0} \approx \phi^{-1.75} \quad (16)$$

If the excluded volume interactions are taken into account, slightly different exponents of the above scaling laws are

SCHEME 1: Molecular Structure of C₈F₁₇EO₁₀

obtained. For branched or interconnected micelles, the exponents of the scaling laws are significantly different.^{48,49} For example, $G''_{\text{min}}/G_0 \approx \phi^{-0.75}$ has been proposed for a saturated interconnected network.^{10,50}

Experimental Section

Materials. The fluorinated surfactant perfluoroalkyl sulfonamide ethoxylate, C₈F₁₇SO₂N(C₃H₇)(C₂H₄O)₁₀H, designated as C₈F₁₇EO₁₀ (Scheme 1) was obtained from Mitsubishi Materials (Japan). The surfactant was purified by placing it under vacuum for several days to remove volatile components until the weight became constant. The surfactant was used without further purification. Millipore water was used in all the experiments.

Phase Diagram. For the study of phase behavior, sealed ampules containing required amount of reagents were homogenized and kept in a water bath for equilibration. Liquid crystalline samples were characterized by visual observation (through crossed polarizers) and also by SAXS.

Rheological Measurements. Samples for rheological measurements were homogenized and kept in a water bath at 25 °C for at least 24 h to ensure equilibration before performing measurements. The rheological measurements were performed in an ARES rheometer (Rheometric Scientific) using couette geometry. The temperature was controlled with circulating fluid from a temperature-controlled water bath. A sample cover provided with the instrument was used to minimize the change in sample composition by evaporation during the measurement. While studying the effect of temperature on the rheological behavior, we maintained the samples at each temperature from 30 min (for samples of low viscosity) to 1 h (for samples of high viscosity) before the measurements, which was sufficient to attain a stability in the rheological parameters (η and G_0), as suggested by a separate rheological measurement as a function of time. Frequency sweep measurements were performed in the linear viscoelastic regime of the samples, as determined previously by dynamic-strain sweep measurements. The zero-shear viscosity of the samples was determined either from a steady shear rate measurement of less viscous samples by extrapolating the viscosity (shear-rate curve to zero-shear rate) or from the values of G_0 and τ_R as obtained from oscillatory measurements (eqs 7 and 8).

SAXS. SAXS measurements on micellar solutions were performed by a SAXSess camera (Anton Paar) equipped with the PW3830 laboratory X-ray generator operating at 40 kV and 50 mA, a long fine-focus sealed-glass X-ray tube (K α wavelength of 0.1542 nm) from PANalytical, focusing multilayer optics, a block collimator for a slit collimation, a translucent beam stop, an image plate (IP) detector, and a temperature-controlled sample holder unit (TCS 120, Anton Paar). The sample was taken in a clean capillary, and the same capillary was repeatedly used for all measurements. The scattered intensity recorded on the IP was read by means of a Cyclone storage phosphor system (Perkin-Elmer). Because of the translucent beam stopper, the raw scattering data always included a reduced primary intensity at a scattering vector $q = 0$. All the data were normalized to the same incident primary-beam intensity for the transmission calibration and were corrected for the background scattering from the capillary and the solvent. The absolute scale calibration was done using water as a secondary standard. The maximum resolution of the instrument,

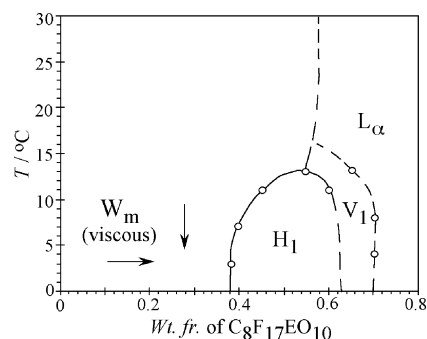


Figure 2. Partial phase diagram of C₈F₁₇EO₁₀/water binary system. W_m stands for the micellar solution, and H₁, V₁, and L_α stand for hexagonal, bicontinuous cubic, and lamellar liquid crystalline phases. The arrows in the W_m domain show the direction the of viscosity increase for the systems at surfactant concentration of 15 wt % and above. At lower concentrations, viscosity increases and then decreases with increasing temperature. For details, see Figure 6.

q_{min} , was $\sim 0.08 \text{ nm}^{-1}$, which corresponds to ~ 40 and $\sim 80 \text{ nm}$ for the detectable maximum size of a particle and interlayer spacing, respectively.

The primary SAXS data were analyzed by the GIFT technique with the Boltzmann simplex simulated annealing (BSSA) algorithm. In the calculation, we used a model of the averaged structure factor for a hardsphere (HS) interaction, $S(q)^{\text{av}}$, which considers the Gaussian distribution of the interaction radius, σ , for individual monodisperse systems for polydispersity, μ , and a Percus–Yevick (PY) closure relation to solve Ornstein–Zernike (OZ) equation.^{51,52} The detailed theoretical description on the method has been reported elsewhere.^{31,33}

DLS Measurements. Dynamic light-scattering measurements were performed in homodyne light-beating mode with vertically polarized light from a diode laser operated at 200 mW CW and 532 nm wavelength on an ALV SP-86 goniometer equipped with a photomultiplier detector operated in photon-count mode in the far field. The scattered light intensity's autocorrelation function, $g(t)$, was accumulated by an ALV5000 correlator. Thermostated, $> 6 \text{ h}$ -annealed, samples taken in cylindrical glass cells were used in the measurement.

Results and Discussion

Phase Behavior. The phase diagram of the C₈F₁₇EO₁₀/water binary system is shown in Figure 2. This is a typical phase diagram of a nonionic surfactant, such as polyoxyethylene alkyl ethers (C_mEO_n),⁵³ with a close resemblance to the phase diagram of C₁₂EO₆. At low-temperature, a micellar solution is formed over a wide range of compositions (up to $\sim 38 \text{ wt } \%$ at 5°C). With a further increase in surfactant concentration, hexagonal (H₁), bicontinuous cubic (V₁), and lamellar (L_α) liquid crystalline phases are formed successively. Micellar solutions at low temperature become increasingly viscous with increasing surfactant concentration, and at compositions near the H₁ phase, a highly viscous or gel-like solution is formed. However, the SAXS pattern shows a broad scattering band (data not shown), which rules out the possibility of the presence of the discontinuous cubic (I₁) phase. Moreover, the fact that the viscosity of the solution gradually increases with increasing concentration also indicates that the I₁ phase is not present. In fact, the formation of globular micelles is not favorable because of bulky and stiff fluorinated chain unless the headgroup is very big. With increasing temperature, the viscosity of the solution gradually decreases, and ultimately, a less viscous easily flowing isotropic solution is formed. At higher temperatures, a phase separation occurs which is typical of nonionic surfactant

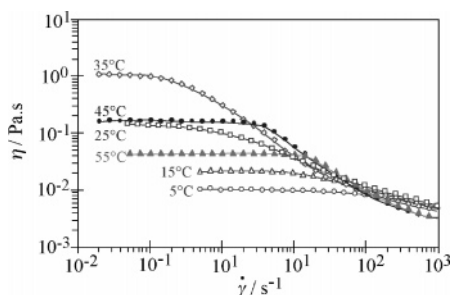


Figure 3. Steady-shear -rate ($\dot{\gamma}$) vs viscosity (η) curves of a 1 wt % surfactant system at various temperatures.

systems. The phase diagram of this system over wide range of temperatures and compositions has been reported recently.⁵⁴ Although the present diagram is essentially similar to the reported diagram, the H_1 melts at lower temperature in the present diagram. We believe that the discrepancy is related to the purity of the surfactant sample because small amount of impurities affect the phase behavior significantly.

Steady-Shear Rheological Behavior. Figure 3 shows the steady shear rate ($\dot{\gamma}$) versus viscosity (η) curves for 1 wt % surfactant solution at different temperatures. At low temperature (5 °C), η is independent of $\dot{\gamma}$ (i.e., Newtonian flow behavior is observed up to $\dot{\gamma} \approx 100 \text{ s}^{-1}$). At higher values of $\dot{\gamma}$ ($> 100 \text{ s}^{-1}$), the viscosity decreases with increasing $\dot{\gamma}$, and this “shear-thinning” behavior can be described by the power law: $\eta \propto \dot{\gamma}^{-a}$. This behavior is typical of wormlike micelles. Note that the viscosity of the surfactant solution is significantly higher than that of water or micellar solutions generally observed in surfactant solutions at such a low concentration of 1 wt %. Therefore, cylindrical micelles are expected to be present even at low temperatures. Upon an increase of the temperature up to 35 °C, the plateau value of η at low $\dot{\gamma}$ (and hence η_o) increases, and the shear thinning also begins at a lower-shear rate, with nearly similar value of exponent in the power law. It suggests that the system is getting more “structured” with increasing temperature. When the temperature is increased further to 45 °C, η at low- $\dot{\gamma}$ (or η_o) decreases, and the critical shear rate shifts again to higher values, but η decreases more steeply with $\dot{\gamma}$ (larger a in the power law) than was observed at lower temperatures. A comparison of the steady shear-rate curves at 25 and 45 °C shows that, although the viscosity at low $\dot{\gamma}$ (plateau value) is nearly same, the shear-thinning behavior at higher-shear rate is not similar, which might be the result of a difference in the structure of the system at the respective temperatures. Rheological measurement was carried out only up to 55 °C because phase separation occurs at higher temperature.

The increase in η_o with temperature in the nonionic surfactant can be understood in terms of the decrease in a_s or the decrease in the interfacial curvature of aggregates because of the progressive dehydration of the EO chain. This would induce a sphere-rod transition in the aggregate shape or induce one-dimensional growth if the rodlike aggregates are already formed. The formation of end caps in the cylindrical aggregates becomes unfavorable with increasing temperature because of the high free-energy cost of formation of hemispherical ends and consequently one dimensional growth is favored. The trend observed up to 35 °C is consistent with that view. However, above 35 °C, a turning point occurs, and the viscosity begins to decrease as if the micellar length changes in opposite direction for some reason, such as an increase in the extent of micellar scission kinetics. A more convincing explanation is that with increasing temperature, the energy cost of the free ends of the micelles become higher, and therefore, the free ends would fuse

at the cylindrical part of its own or of another micelle, thus forming micellar joints or branching.^{9,55} Such joints reduce the viscosity because, when a stress is applied, the micellar joint can slide along the cylindrical body (contour) thereby allowing a fast stress relaxation process. Since the surfactant molecules in the aggregate are not chemically connected, the surfactants are expected to form this type of saddle-shaped interconnection readily if they do not strongly resist a negative Gaussian curvature. Micellar connections or branching have been detected by cryogenic transmission electron microscopy (cryo-TEM) in some surfactant systems, especially in the region where the viscosity decreases after the maximum.^{56–59} In recent years, a theoretical basis for the formation of branching and network, supported by experimental evidence, has been provided.^{60–62}

SAXS. To study the variation of microstructural changes in the shape and size of aggregates as a function of temperature, SAXS measurements were performed on a 1 wt % surfactant solution at different temperatures (viz., 15, 35, 45, and 55 °C). As can be seen from Figure 3 (and also from Figure 6), these temperatures correspond to the different regions of the viscosity temperature curves, namely, viscosity-growth region, viscosity-maximum region, viscosity-decline region after the maximum, and near the phase boundary, respectively. Figure 4 shows the $I(q)-q$ curves after the correction for instrumental broadening (desmearing). The absence of a peak or maximum in the low- q region indicates a negligible interparticle interaction. In fact, the analysis of data without consideration of structure factor (using the IFT method) gave nearly identical results. The decay of $I(q)$ at $\sim q^{-1}$ in the low- q region suggests that the aggregates have rodlike local structures at 15, 35, and 45 °C. However, at 55 °C, a very small but noticeable increase in the slope in the $q < 0.7 \text{ nm}^{-1}$ region was observed which suggests that the aggregate shape is mainly cylindrical but a lamellarlike structure is gradually developing. Lamellarlike aggregates are characterized by $I(q)$ decaying at $\sim q^{-2}$ in the low- q region. The structural change with increasing temperature is more evident from the corresponding PDDF curves shown in Figure 4. The pattern of the PDDF plots at 15, 35, and 45 °C are typical of rodlike particles (see Figure 1). The PDDFs of the aggregates show that the D_{max} increases with increasing temperature, but the cylindrical cross-sectional diameter of the rodlike aggregates is almost constant ($\sim 5.8 \text{ nm}$). Note that the measured value of D_{max} is biased by the maximum of resolution (or q_{min}) of the measurement, and it may not provide the actual length of the micelles, which are believed to have their contour lengths in the several hundred nanometers or even micrometer range. Nevertheless, the trends in the variation of D_{max} values as obtained from SAXS measurements can be taken as the evidence of micellar growth.

Further information on the structure of the aggregates can be obtained from the SAXS data. Figure 5 shows the representative cross-sectional PDDF, $p_c(r)$, considering the long cylindrical shape of the aggregate and the radial contrast profile, $\Delta\rho_c(r)$, of the cross-section as obtained by deconvolution of $p_c(r)$. The cross-sectional radius of the aggregate is estimated to be $\sim 2.95 \text{ nm}$, which corresponds to half of the value of r for $p_c(r) = 0$ at large r (shown by an arrow in Figure 5). An extended length of 1.7 nm is estimated for the $\text{C}_8\text{F}_{17}\text{-S-N}$ moiety with a rigid fluorocarbon chain. This value is consistent with the experimental value of 1.8 nm reported for the radius of the hydrophobic core of cylindrical aggregates (H_1 phase) formed by a perfluorosurfactant $\text{C}_8\text{F}_{17}\text{C}_2\text{H}_4\text{EO}_9$,⁶³ which has a hydrophobic moiety of a length comparable to that of the surfactant of present study. With this, $\sim 1.2 \text{ nm}$ is left for the length of

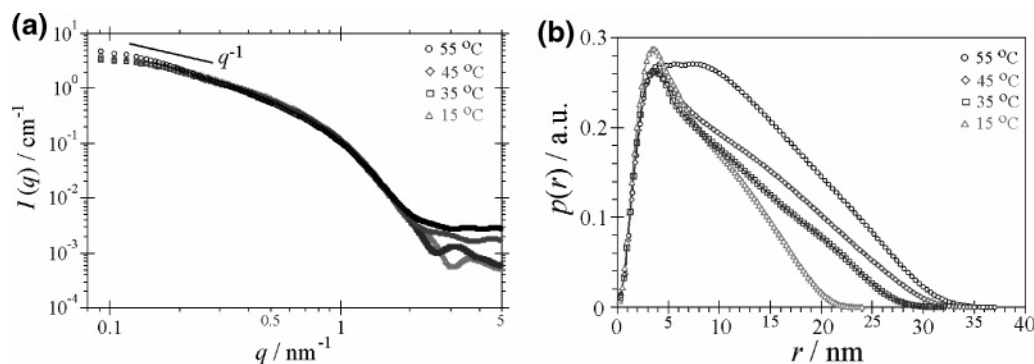


Figure 4. Scattered intensity, $I(q)$, from an SAXS measurement of a 1 wt % surfactant solution at different temperatures (a). Corresponding pair-distance distribution functions, $p(r)$, are shown in panel b.

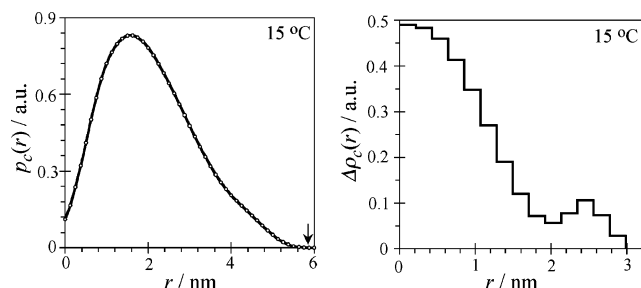


Figure 5. Cross sectional PDDF, $p_c(r)$, and contrast profile, $\Delta\rho_c(r)$, as obtained from the deconvolution of $p_c(r)$ for a 1% surfactant system at 15 °C. Scattering intensity curve is shown in Figure 4.

hydrophilic chain (EO₁₀) of the surfactant. The lengths of the EO₁₀ chain are 1.8–2.0 and 3.5 nm in the meander and zigzag configurations, respectively. A zigzag conformation has been suggested for EO chains of less than 18–20 EO units. The estimated length of an EO₁₀ chain with a zigzag configuration is nearly three times longer than the value estimated from the PDDFs. Even if we assume a meander configuration, the length of the EO chain obtained from the PDDFs is not consistent with the reported length. Note that the zigzag conformation cannot be ruled out just because of the observed discrepancy in the EO chain length because the contrast of the EO chain is low and it gradually decreases further when the EO units extend toward the solvent (water). An increase in the extent of hydration further decreases the contrast and makes the estimation of the correct length of the EO chain impossible. The extended part of the $p_c(r)$ curve in the higher- r region (Figure 5) probably comes from the fading contrast profile outside the fluorinated core, although a noncircular cross-section may also introduce asymmetry in the $p_c(r)$ plot. Assuming a circular cross-section of the cylindrical aggregates, a contrast step profile was obtained by deconvolution, and the result is shown in Figure 5. The fluorocarbon core has a high-electron density and, therefore, shows a high contrast. A minimum in the contrast profile is observed around $r = 2$ nm. It is reasonable because the $-C_3H_7$ moiety of the low-electron density might have balanced the positive contribution of N, S, and O, bringing the overall contrast profile to a low value. With increasing r values, the contrast profile improves slightly, which is due to EO chain, but it fades out gradually and eventually approaches to zero.

The results of SAXS measurements, especially the constant cross-sectional diameter and increasing D_{\max} , provide important information about the microstructural changes. The continuity in the one-dimensional micellar growth even above 35 °C, which is the $T_{\eta-\max}$ for the system, confirms that the decay of the viscosity above this temperature is not caused by decreases in the length of the cylindrical aggregates. With a further increase

in temperature to 55 °C, the D_{\max} continues to increase, but more importantly, there is the significant change in the pattern of $p(r)$ observed in the middle- r region (Figure 4). Here, a sharp decay of $p(r)$ immediately after the maximum has healed, and a significant bulge in upward direction has developed in that region. In fact, careful analysis of the evolution of the $p(r)$ curves reveals that indication of such a change has already begun at 45 °C, although to a small extent. Such a change in the $p(r)$ would suggest a gradual evolution of the local structure toward a lamellar pattern⁶⁴ (see Figure 1). With a gradual evolution of the lamellar structure (with increasing temperature), we can expect that the bulge at the intermediate- r region would grow and, ultimately, that the maximum in the low- r region would completely disappear and the $p(r)$ curve would transform to a bump with a broad maximum in the intermediate- r region, which is a typical pattern for a flat structure (Figure 1). SAXS measurements were not carried out at higher temperature. Therefore, evidence of the evolution of the aggregate shape to form a locally flat structure is not available. Even from the scattering pattern from SAXS and corresponding $p(r)$ curves, it is not possible to distinguish among different structures such as vesicles, lamellar liquid crystalline (L_α) phases, or sponge (L_3) phases.

Temperature-induced micellar growth and evolution of low curvature structures at elevated temperature as shown by SAXS measurements provide a direct evidence of the formation of micellar joints or branching. At branching points, the mean local curvature is zero. Probably the number and size of those points grows sharply with increasing temperature at $T > T_{\eta-\max}$. In dilute solutions of several ionic as well as hydrophilic nonionic surfactants successive addition of lipophilic nonionic surfactant such as C₁₂EO₃ induces one-dimensional micellar growth and causes the viscosity to sharply increase to a maximum and then decrease. Ultimately, a two-phase region consisting of aggregates with low curvature (L_α phase or vesicles) and micellar solution appears. Still it is not clearly understood how wormlike micelles transform to structures with very low curvature. Most probably, formation of micellar joints and the growth of the joints to a bilayer structure is the mechanism. It is reasonable to expect a similar type of structural evolution in the present system because increasing temperature and the addition of a lipophilic surfactant both decrease the interfacial curvature of the aggregates.

Effect of Surfactant Concentrations on Viscosity. Figure 6 shows the variation of η_0 as a function of temperature at different compositions, including the 1 wt % surfactant system described above. At 0.5 wt % surfactant concentration, the viscosity of the solution is low, and a gradual but small increase in viscosity is observed with increasing temperature up to 40

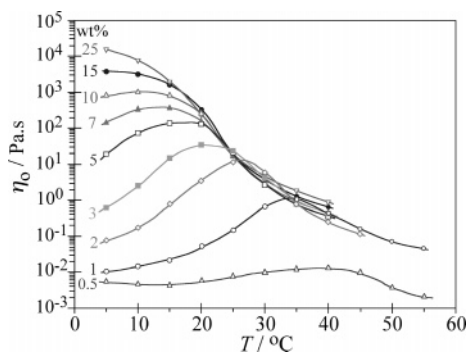


Figure 6. Variation of zero-shear viscosity (η_0) as a function of temperature at different concentrations (in wt %) of surfactant in water.

°C; then it decreases with a further increase in temperature and ultimately a phase separation takes place. With a slight increase in the surfactant concentration (1 wt %), the increase in viscosity with an increase in temperature is clearly visible, with an increase of about 2 orders of magnitude in viscosity upon increasing temperature from 5 to 35 °C. With a further increase in temperature, the viscosity decreases. On the other hand, with an increase in the surfactant composition, the trend of the viscosity–temperature curve is essentially similar, but the temperature for the viscosity maximum ($T_{\eta-\max}$) gradually shifts to a lower value, and there is a significant increase in the viscosity at temperatures below $T_{\eta-\max}$. At a high concentration of surfactant, highly viscoelastic solutions are formed at low temperatures. At a surfactant concentration of 25 wt %, the viscosity decreases with increasing temperature from 5 °C, and judging from the trends of curves, $T_{\eta-\max}$ is well below 5 °C, but the behavior is essentially the same as that observed at lower concentrations. As can be seen from viscosity–temperature curves, the viscosity of the micellar solution is very sensitive to the concentration at low temperatures, but at and above 25 °C, the viscosity is nearly same over a wide range of concentrations (2–25 wt %).

With increasing surfactant concentration, the degree of hydration of the EO chain decreases, and consequently, the aggregation number increases, in addition to the increase in the number density of the aggregates. The decrease in hydration would decrease the spontaneous curvature of the aggregate and, therefore, induce a large energy cost for end-cap formation. These factors would favor one-dimensional micellar growth and, therefore, increase the viscosity. Therefore, the effect of increasing surfactant concentration is similar to that of increasing temperature. Upon an increase of the surfactant concentration, the formation of micellar joints is expected to take place at lower temperature, which can explain the gradual shift of $T_{\eta-\max}$ toward lower temperature.

Oscillatory-Shear Rheological Behavior. Oscillatory-shear (frequency-sweep) measurements were performed on the viscoelastic samples formed around the viscosity maximum. Figure 7 shows a plot of the elastic modulus (G') and loss modulus (G'') as a function of oscillatory-shear frequency (ω) for a sample of a 10% surfactant system at 15, 20, and 25 °C. The result shows that sample is viscoelastic in the time scale of measurement: $G'-G''$ crossover occurs in the low-frequency region at 15 °C. In the low- ω region, the data points of G' and G'' could be fitted to Maxwell equations, but in the high- ω region, the experimental data deviate from the model, which is generally considered to be caused by faster relaxation processes, such as Rouse modes. Maxwellian-type oscillatory rheological behavior of viscous micellar solutions, such as that shown in Figure 7, can be related to the transient network formed by the

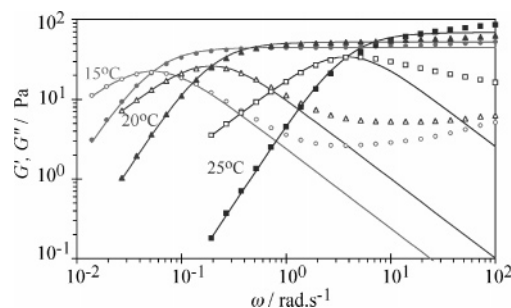


Figure 7. Variation of elastic modulus, G' (filled symbols), and viscous modulus, G'' (open symbols) as a function of oscillatory-shear frequency (ω), obtained by frequency in a 10% surfactant system at different temperatures. Fittings to the Maxwellian equations are shown by solid lines.

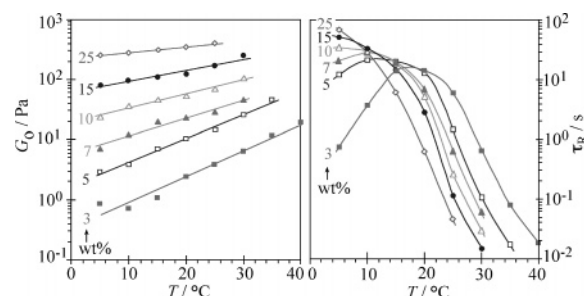


Figure 8. Variation of shear modulus (G_0) and stress relaxation time (τ_R) as a function of temperature at different surfactant concentrations (in wt %).

entanglement of wormlike micelles. The data at lower temperatures have not been shown here for the sake of clarity, but they follow a similar trend. It can be seen from the figure that with increasing temperature the plateau value of G' increases which corresponds to an increase in network density. The $G'-G''$ crossover frequency shifts to the high-frequency region that suggests faster relaxation processes resulting from the formation of micellar joints, but the network density also increases as indicated by an increase in G' plateau.

The rheological parameters G_0 and τ_R may be obtained by fitting of the experimental data from frequency-sweep measurements, especially the data in low-frequency region, to the Maxwell equations. As in the case of the system described in Figure 7, G' at the high- ω region (say G'_∞) usually does not attain a perfect plateau as predicted by the Maxwell equations. Instead, G'_∞ is often higher than the value of G_0 given by the Maxwell model. Therefore, the values of G_0 estimated from Maxwell equations should be considered as the lower limit for the shear modulus. Figure 8 shows the variation of G_0 and τ_R as a function of temperature at different surfactant concentrations. It can be seen that G_0 increases monotonically with increasing temperature, which may be taken as the evidence of a one-dimensional micellar growth and, consequently, of an increase in the density of the entanglements of the wormlike micelles with increasing temperature at all concentrations. However, the extent of the increase of G_0 with temperature decreases with increasing surfactant concentration. At a 3 wt % surfactant concentration, G_0 increases by 1 order of magnitude when temperature changes by 20 °C, whereas at 25 wt % the change is significantly small. At high concentrations, G_0 could not be ascertained at higher temperature because the $G'-G''$ crossover occurs very near or above the upper working limit of ω of the instrument. Nevertheless, it can be expected from the trend that the behavior is likely to be similar at higher temperatures as well.

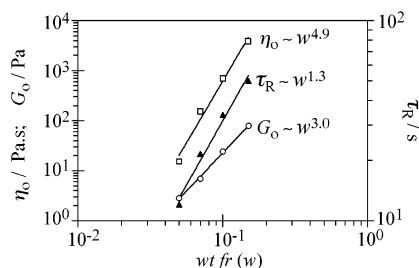


Figure 9. Variation of η_0 , G_0 , and τ_R as a function of surfactant weight fraction (w) at 5 °C. The scaling relations of each of the parameters are shown next to the corresponding data series. For the scaling relations at other temperatures, see the text.

On the other hand, the τ_R of the viscoelastic solutions at low concentrations, for example, in a 3 wt % surfactant system, first increases swiftly with increasing temperature, reaches the maximum value at ~ 20 °C, and then decreases (Figure 8). Upon an increase of the surfactant concentration from 3 to 5 wt % and above, the trend remains essentially same, but the position of the τ_R maximum gradually shifts to lower temperature. At higher concentrations of surfactants (e.g., at 10 and 15 wt %), the τ_R maxima are around 5 °C. At a surfactant concentration of 25 wt %, no maximum is seen, but τ_R decreases from 5 °C. However, judging from the trends of the τ_R – T curves, the τ_R maxima for these concentrations is expected to fall below 5 °C. Nevertheless, τ_R approaches a very large value (e.g., ~ 67 s) for a 25 wt % system at 5 °C, which corresponds to the presence of very long micelles.

The observed trend in τ_R clearly shows that with increasing temperature some structural changes occur in the network which allow the system to release the stress quickly. The shortening of the micelles is ruled out because the monotonic increase in G_0 clearly indicates that network density increases with temperature. These results are consistent with the formation of micellar joints or branching because sliding of the branching point along the micellar length can provide a fast stress relaxation mechanism.

The scaling relationship of different rheological parameters with the volume fraction of surfactant (ϕ) is based on the uncharged polymer solution. The validity of scaling relationships to the wormlike micellar system has been tested only in the systems of ionic surfactants in the presence of counterions. The present nonionic surfactant system would be an appropriate system to check the validity of the scaling relationships. Figure 9 shows the variation of η_0 , G_0 , and τ_R with the weight fraction of the surfactant in the system (w) at fixed temperature (5 °C). Since w is proportional to ϕ , the exponents of the scaling relationships can be evaluated from such plots. Note that systems with branched micelles have lower values of viscosity and relaxation time than those of the systems of unbranched micelles, and therefore, they exhibit different scaling behavior. Hence, the data points corresponding to a 25 wt % system have not been included in the plot shown in Figure 9. The exponents of η_0 and G_0 evaluated from the experimental data are larger than the theoretical values, whereas the exponent of τ_R is very close to the theoretical value. The exponents of the power laws decrease with increasing temperature. Scaling relationships with lower values of exponents (viz., $\eta_0 \approx w^{3.4}$, $G_0 \approx w^{2.9}$, and $\tau_R \approx w^{0.4}$ at 10 °C and $\eta_0 \approx w^{2.2}$, $G_0 \approx w^{2.5}$, and $\tau_R \approx w^{-0.3}$ at 15 °C) come from the increase in the number density of the micellar joints and the gradual shift toward the formation of saturated network.

Figure 10 shows the variation of G''_{\min}/G_0 with temperature at surfactant concentrations of 7, 10, and 15 wt %. At higher

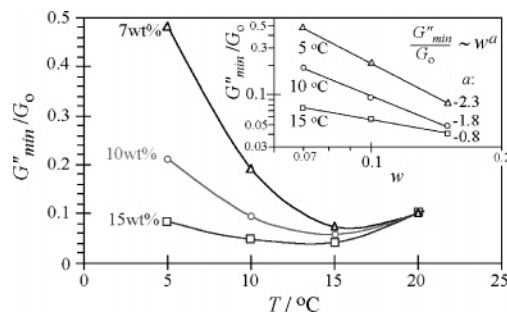


Figure 10. Variation of G''_{\min}/G_0 as a function of temperatures at different surfactant concentrations. The plot of G''_{\min}/G_0 as a function of the weight fraction of surfactant, w , at different temperatures is shown in the inset.

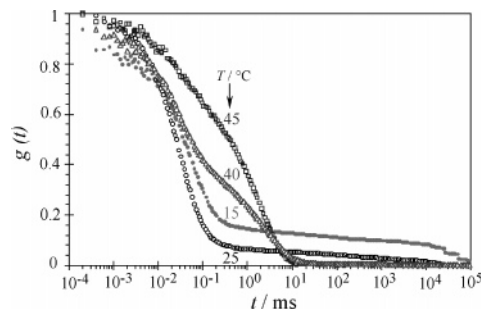


Figure 11. Normalized autocorrelation function, $g(t)$, for different temperatures in a 5 wt % EF122B aqueous systems. The detection angle is 90°.

temperature (>20 °C) and lower surfactant concentrations, not enough data points are available because the minima in the G'' could not be obtained within the frequency range of measurement, and therefore, G''_{\min}/G_0 are not available. At a surfactant concentration of 7 wt %, the parameter decreases with increasing temperature up to 15 °C, which corresponds approximately to $T_{\eta-\max}$ for the series, and then increases. The minimum becomes increasingly shallow with increasing concentration and shifts gradually to the lower temperature. The minimum corresponds to the related minimum in l_e/\bar{L} . The parameter l_e and, from there, \bar{L} can be estimated provided that l_p is known. However, l_p is not available for the fluorinated nonionic surfactant system. If we assume that l_e is approximately constant within the range of temperature (5–20 °C), the minimum in G''_{\min}/G_0 corresponds to the maximum in \bar{L} .

The variation of G''_{\min}/G_0 as a function of weight fraction of surfactant at 5 °C, as well as at higher temperatures (10 and 15 °C), is shown in the inset of Figure 10. It can be seen that the power-law exponents are temperature dependent. The magnitude of the exponent decreases with increasing temperature, and it approaches to zero at 20 °C; although the plot at this temperature is not shown in the inset for the sake of clarity, it is clearly evident from the G''_{\min}/G_0 versus T plot. The decrease in the exponent is related to the formation of micellar joints or branching.⁶⁵ The experimental values of the power-law exponent at 10 and 15 °C are very close to the theoretical values proposed for linear and saturated aggregates, respectively,^{10,48–50} but at 5 °C, the experimental value is higher than the predicted value.

DLS. DLS is commonly used as a complementary technique for the study of viscoelastic solutions. As shown in Figure 11, in the present system, the normalized autocorrelation function, $g(t)$, shows several decays that can be attributed to different relaxation processes, as typically found in wormlike micellar systems. At 15 °C, $g(t)$ becomes zero at very long times, almost out of the experimental window, indicating that the system is

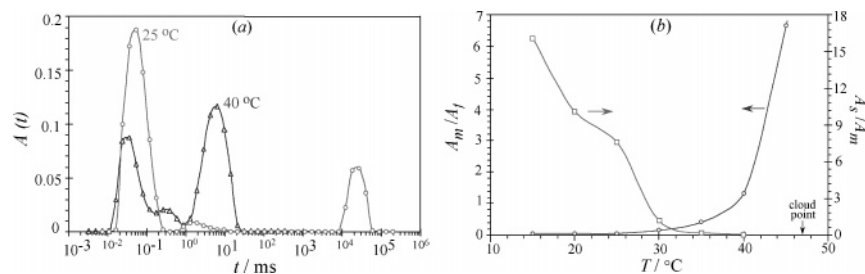


Figure 12. Distribution of relaxation times estimated by the CONTIN method in a 5 wt % EF122B aqueous system at different temperature. The detection angle is 90° (a). Relative contributions of fast (A_f), medium (A_m), and slow (A_s) modes to the distributions of relaxation times as a function of temperature (b). The continuous lines are only for visual guide.

somewhat “frozen” and nearly nonergodic. In fact, the slow relaxation times diverge at the gel point.⁶⁶ However, the time for which $g(t) = 0$ tends to shift to lower values as the temperature is increased over 25 °C, indicating faster relaxation, which is in agreement with the change of viscoelastic properties with temperature presented in previous sections. At 45 °C, near the surfactant cloud point at the given concentration, the shift of the fast decay to the right becomes evident. A similar behavior has been found in other nonionic wormlike micelles⁶⁴ and was attributed to the formation of structures with low curvature. But in the present case, there is an additional factor, which is the onset of attractive interactions as nonionic surfactants approach the cloud point.⁶⁷ The general trend of Figure 11 is different from other nonionic micellar systems which form globular micelles at low temperatures and give $g(t)$ values that can be closely fitted by single exponentials.⁶⁴

As can be seen in Figure 12a for two representative temperatures, the CONTIN analysis of $g(t)$ gives three relaxation modes, similar to other systems in which wormlike micelles are present.^{27,68–71} At temperatures below 25 °C, it is difficult to define precisely the distribution peak corresponding to the slow mode because the associated relaxation time is very long and falls out of the experimental limit. At low temperatures, the fastest mode is also the one with the highest contribution to the distribution of relaxation times. It was found that the inverse of the relaxation time associated with this mode changes linearly with the square of the scattering vector, namely, $\tau^{-1} = Dq^2$, where D is the diffusion coefficient. In other words, the fastest mode is diffusive and may be attributed to the diffusion of micelles. Moreover, the peak maximum of this mode corresponds to a hydrodynamic length (estimated by the Stokes–Einstein equation) that shows some increase (from 4 to 6 nm) with temperature from 15 to 40 °C. It is known that nontangled nonionic micelles show strong micellar growth as temperature is increased.^{67,72,73} It is interesting to note that the mentioned length is similar to that obtained for the cross-sectional diameter of micelles according to the SAXS calculations. With consideration of the polydispersity of the wormlike micellar systems, it has been argued that fast modes in wormlike micellar systems might correspond to the diffusion of aggregates with low-axial ratios, which coexist with long micelles.^{27,68} This coexistence has already been confirmed for ionic fluorosurfactants by transmission electron microscopy (TEM)¹⁷ and inferred from the DLS measurements.⁷⁴ Accordingly, small aggregates would have a size close to the diameter of hemispherical end caps of the wormlike micelles.

The other two modes (medium and slow) at low temperatures do not follow the linear τ^{-1} versus q^2 relationship, and therefore they cannot be considered diffusive. This is in agreement with previous reports on wormlike micelles.^{70,71} The range of distribution times covered by the medium mode are in the same scale of the lifetime of transient connections between wormlike

micelles found by Kato⁷⁵ and other authors.^{70,71} The medium mode is theoretically predicted for entangled polymer solutions and has been assigned to the Rouse mode,⁷⁶ which is estimated to be smaller than the slow reptational mode, as in the present case at low temperatures. However, this is not always the case.⁷⁰ From the position of the medium mode, values of hydrodynamic length ranging from 1 to 2 μm are estimated, namely, the change with temperature is not very large. However, as the temperature is increased, the medium mode prevails over the fastest mode, and the third mode tends to disappear. To better illustrate this point, the relative the contributions of fast (A_f), medium (A_m), and slow (A_s) modes to the distributions of relaxation times as a function of temperature are plotted as A_m/A_f and A_s/A_m in Figure 12b. The fact that the medium mode is by far the most significant at high temperatures, as expressed by the increase in A_m/A_f ratio, indicates that it is related to large structures, probably having junctions that are not stable enough to generate a slow relaxation mode. This would be in agreement with the formation of branched aggregates and the resultant loss of viscoelastic properties at high temperatures. Note the sharp increase of the A_f/A_m ratio as the system approaches the cloud point and the onset of micellar interactions.

On the other hand, the decrease in the contribution of the fast mode could indicate that small aggregates have been converted to larger ones with the increase in temperature. Another possibility is that this mode is also related in some way to the micellar end caps, the number of which would decrease as micellar joints and branches are formed to decrease the energy penalty derived from the unfavorable curvature of those caps.

Although it should be mentioned again that there are some inaccuracies in the determination of the amplitude and position of the distribution peak related to the slow mode at low temperatures because of the time scale of the experiment, there is a correlation between the decrease in the A_s/A_m ratio and the decrease in viscosity and the loss of viscoelastic properties as temperature is increased, which supports the assignment of this mode to the presence of long-range networks.⁷⁷

Summary

Fluorinated surfactants tend to form aggregates with low curvature, such as cylindrical aggregates, at a solution conditions where hydrocarbon surfactants would form spherical aggregates. A nonionic fluorinated surfactant, perfluoroalkyl sulfonamide ethoxylate, forms flexible cylindrical aggregates in water even at low-surfactant concentrations and low temperature, and with an increase in the surfactant concentration, these cylindrical micelles undergo one-dimensional growth and form very long and flexible wormlike micelles which entangle and form a network making a viscoelastic solution. The dynamic rheological behavior can be described by the Maxwell model at low-shear

frequency, which is typical behavior of wormlike micellar solution. With successive increases in the surfactant concentration, the aggregates lose the flexibility and transform into hexagonal liquid crystalline phases. An increase in the temperature of the nonionic surfactant system reduces the interfacial curvature and induces micellar growth, which is mainly attributed to the progressive increase in the energy cost for the formation of the hemispherical end caps of the aggregates. Therefore, the viscosity increases with temperature. Above a certain temperature, viscosity begins to decrease, not because of the shrinking of micelles but because the system tends to eliminate the free ends by forming micellar joints in the network and such changes in the microstructure result in a decrease in the viscosity and stress relaxation time, but the network structure is retained. Variations of the rheological parameters are in agreement, and SAXS provides a direct evidence of such microstructural changes. The temperature at which the viscosity begins a decline shifts gradually toward lower values when the surfactant concentration increases because both have similar effects on the interfacial curvature. The rheological parameters, η_0 and G_0 , show scaling relationships with surfactant concentrations with exponents greater than the values predicted by the living-polymer model, but the exponent of τ_R is in agreement with the theory. Finally, DLS measurements indicate the presence of fast-relaxation modes, associated with micelles, and medium and slow modes, associated with transient networks. The disappearance of the slow mode and the predominance of the medium mode as the temperature is increased give support to the conclusions derived from SAXS and rheometry.

Acknowledgment. This work was supported by CREST of Japan Science and Technology Corporation. D.P.A. thanks the Japan Society for the Promotion of Science (JSPS) for financial support. This work is dedicated to Prof. Hironobu Kunieda who inspired the authors to carry out this work but passed away before the work was finalized.

References and Notes

- (1) Shinoda, K.; Hato, M.; Hayashi, T. *J. Phys. Chem.* **1972**, *76*, 909–914.
- (2) Kunieda, H.; Shinoda, K. *J. Phys. Chem.* **1976**, *80*, 2468–2470.
- (3) Israelachvili, J. N.; Mitchell, D. J.; Ninham, B. W. *J. Chem. Soc., Faraday Trans. 2* **1976**, *72*, 1525.
- (4) Tanford, C. *The Hydrophobic Effect: Formation of Micelles and Biological Membranes*, 2nd ed.; John Wiley & Sons: New York, 1980.
- (5) El Moujahid, C.; Ravey, J. C.; Schmitt, V.; Stébé, M. *J. Colloid Surf. A* **1998**, *136*, 289–297.
- (6) Rehage, H.; Hoffmann, H. *J. Phys. Chem.* **1988**, *92*, 4712–4719.
- (7) Kern, F.; Lemarchal, P.; Candau, S. J.; Cates, M. E. *Langmuir* **1992**, *8*, 437–440.
- (8) Clausen, T. M.; Vinson, P. K.; Minter, J. R.; Davis, H. T.; Talmon, Y.; Miller, W. G. *J. Phys. Chem.* **1992**, *96*, 474–484.
- (9) Khatory, A.; Kern, F.; Lequeux, F.; Appell, J.; Porte, G.; Morie, N.; Ott, A.; Urbach, W. *Langmuir* **1993**, *9*, 933–939.
- (10) Khatory, A.; Lequeux, F.; Kern, F.; Candau, S. J. *Langmuir* **1993**, *9*, 1456–1464.
- (11) Berret, J.-F.; Appell, J.; Porte, G. *Langmuir* **1993**, *9*, 2851–2854.
- (12) Lin, Z.; Cai, J. J.; Scriven, L. E.; Davis, H. T. *J. Phys. Chem.* **1994**, *98*, 5984–5993.
- (13) Soltero, J. F. A.; Puig, J. E.; Manero, O.; Schulz, P. C. *Langmuir* **1995**, *11*, 3337–3346.
- (14) Soltero, J. F. A.; Puig, J. E.; Manero, O. *Langmuir* **1996**, *12*, 2654–2662.
- (15) Narayanan, J.; Manohar, C.; Kern, F.; Lequeux, F.; Candau, S. J. *Langmuir* **1997**, *13*, 5235–5243.
- (16) Hassan, P. A.; Candau, S. J.; Kern, F.; Manohar, C. *Langmuir* **1998**, *14*, 6025–6029.
- (17) Wang, K.; Karlsson, G.; Almgren, M.; Asakawa, T. *J. Phys. Chem. B* **1999**, *103*, 9237–9246.
- (18) Knoblich, A.; Matsumoto, M.; Murata, K.; Fujiyoshi, Y. *Langmuir* **1995**, *11*, 2361–2368.
- (19) Hoffmann, H.; Würtz, J. *J. Mol. Liquids* **1997**, *72*, 191–230.
- (20) Abe, M.; Tobita, K.; Sakai, H.; Kondo, Y.; Yoshino, N.; Kasahara, Y.; Matsuzawa, H.; Iwahashi, M.; Momozawa, N.; Nishiyama, K. *Langmuir* **1997**, *13*, 2932–2934.
- (21) Tobita, K.; Sakai, H.; Kondo, Y.; Yoshino, N.; Iwahashi, M.; Momozawa, N.; Abe, M. *Langmuir* **1997**, *13*, 5054–5055.
- (22) Tobita, K.; Sakai, H.; Kondo, Y.; Yoshino, N.; Kamogawa, K.; Momozawa, N.; Abe, M. *Langmuir* **1998**, *14*, 4753–4757.
- (23) Danino, D.; Weihs, D.; Zana, R.; Örödd, G.; Lindblom, G.; Abe, M.; Talmon, Y. *J. Colloid Interface Sci.* **2003**, *259*, 382–390.
- (24) Acharya, D. P.; Kunieda, H. *J. Phys. Chem. B* **2003**, *107*, 10168–10175.
- (25) Acharya, D. P.; Hossain, Md. K.; Jin-Feng, Sakai, T.; Kunieda, H. *Phys. Chem. Chem. Phys.* **2004**, *6*, 1627–1631.
- (26) Naito, N.; Acharya, D. P.; Tanimura, K.; Kunieda, H. *J. Oleo Sci.* **2004**, *53*, 599–606.
- (27) Maestro, A.; Acharya, D. P.; Furukawa, H.; Gutiérrez, J. M.; López-Quintela, M. A.; Ishitobi, M.; Kunieda, H. *J. Phys. Chem. B* **2004**, *108*, 14009–14016.
- (28) Herb, C. A.; Chen, L. B.; Sun, W. M. In *Structure and Flow in Surfactant Solutions*; Herb, C. A., Prud'homme, R. K., Eds.; ACS Symposium Series 578; American Chemical Society: Washington, DC, 1994; pp 153–166.
- (29) Rodríguez, C.; Acharya, D. P.; Hattori, K.; Sakai, T.; Kunieda, H. *Langmuir* **2003**, *19*, 8692–8696.
- (30) Acharya, D. P.; Hattori, K.; Sakai, T.; Kunieda, H. *Langmuir* **2003**, *19*, 9173–9178.
- (31) Acharya, D. P.; Sato, T.; Singh, Y.; Kunieda, H. *J. Phys. Chem B* **2006**, *110*, 754–760.
- (32) Acharya, D. P.; Shiba, Y.; Aratani, K.-i.; Kunieda, H. *J. Phys. Chem. B* **2004**, *108*, 1790–1797.
- (33) Sato, T.; Hossain, Md. K.; Acharya, D. P.; Glatter, O.; Chiba, A.; Kunieda, H. *J. Phys. Chem. B* **2004**, *108*, 12927–12939.
- (34) Sharma, S. C.; Kunieda, H.; Esquena, J.; Rodríguez-Abreu, C. *J. Colloid Interface Sci.* **2006**, *299*, 297–304.
- (35) Glatter, O. *J. Appl. Crystallogr.* **1977**, *10*, 415–421.
- (36) Glatter, O. *J. Appl. Crystallogr.* **1981**, *14*, 101–108.
- (37) Glatter, O. *Prog. Colloid. Polym. Sci.* **1991**, *84*, 46–54.
- (38) Iampietro, D. J.; Brasher, L. L.; Kaler, E. W.; Stradner, A.; Glatter, O. *J. Phys. Chem. B* **1998**, *102*, 3105–3113.
- (39) Strey, R.; Glatter, O.; Schubert, K.-V.; Kaler, E. W. *J. Chem. Phys.* **1996**, *105*, 1175–1188.
- (40) Brunner-Popela, J.; Glatter, O. *J. Appl. Crystallogr.* **1997**, *30*, 431–442.
- (41) Weyerich, B.; Brunner-Popela, J.; Glatter, O. *J. Appl. Crystallogr.* **1999**, *32*, 197–209.
- (42) Larson, R. G. *The Structure and Rheology of Complex Fluids*; Oxford University Press: New York, 1999.
- (43) Marin, G. In *Rheological Measurement*, 2nd ed.; Collyer, A. A., Clegg, D. W., Eds.; Chapman and Hall: London, 1998.
- (44) Cates, M. E.; Candau, S. J. *J. Phys.: Condens. Matter* **1990**, *2*, 6869–6892.
- (45) Granek, R.; Cates, M. E. *J. Chem. Phys.* **1992**, *96*, 4758–4767.
- (46) Cates, M. E. *J. Phys. Fr.* **1988**, *49*, 1593–1600.
- (47) Berret, J.-F.; Appell, J.; Porte, G. *Langmuir* **1993**, *9*, 2851–2854.
- (48) Drye, T. J.; Cates, M. E. *J. Chem. Phys.* **1993**, *98*, 9790–9797.
- (49) Lequeux, F. *Europhys. Lett.* **1992**, *19*, 675–681.
- (50) Majid, L. J. *J. Phys. Chem. B* **1998**, *102*, 4064–4074.
- (51) Pusey, P. N.; Fijnaut, H. M.; Vrijm, A. J. *J. Chem. Phys.* **1982**, *77*, 4270–4281.
- (52) Salgi, P.; Rajagopalan, R. *Adv. Colloid Interface Sci.* **1993**, *43*, 169–288.
- (53) Mitchell, D. J.; Tiddy, G. J. T.; Waring, L.; Bostock, T.; MacDonald, M. P. *J. Chem. Soc., Faraday Trans. 1* **1983**, *79*, 975–1000.
- (54) Esquena, J.; Rodríguez, C.; Solans, C.; Kunieda, H. *Microporous Mesoporous Mater.* **2006**, *92*, 212–219.
- (55) Candau, S. J.; Oda, R. *Colloid Surf., A* **2001**, *183–185*, 5–14.
- (56) Lin, Z. *Langmuir* **1996**, *12*, 1729–1737.
- (57) Danino, D.; Talmon, Y.; Levy, H.; Beinert, G.; Zana, R. *Science* **1995**, *269*, 1420–1421.
- (58) In, M.; Aguerre-Chariol, O.; Zana, R. *J. Phys. Chem. B* **1999**, *103*, 7747–7750.
- (59) Zana, R. *Adv. Colloid Interface Sci.* **2002**, *97*, 205–253.
- (60) Zilman, A. G.; Safran, S. A. *Phys. Rev. E* **2002**, *66*, 051107.
- (61) Dan, N.; Safran, S. A. *Adv. Colloid Interface Sci.* **2006**, in press.
- (62) Zilman, A.; Safran, S. A.; Sottmann, T.; Strey, R. *Langmuir* **2004**, *20*, 2199–2207.
- (63) Blin, J. L.; Lesieur, P.; Stébé, M. *J. Langmuir* **2004**, *20*, 491–498.
- (64) Moitzi, C.; Freiburger, N.; Glatter, O. *J. Phys. Chem. B* **2005**, *109*, 16161–16168.
- (65) Kern, F.; Lequeux, F.; Zana, R.; Candau, S. J. *Langmuir* **1994**, *10*, 1714–1723.
- (66) Munch, J. P.; Ankrum, M.; Hild, G.; Candau, S. J. *Phys. Lett.* **1983**, *44*, 73.

- (67) Glatter, O.; Fritz, G.; Lindner, H.; Brunner-Popela, J.; Mittelbach, R.; Strey, R.; Stefan U.; Egelhaaf, S. U. *Langmuir* **2000**, *16*, 8692–8701.
- (68) Rodriguez-Abreu, C.; Aramaki, K.; Tanaka, Y.; Lopez-Quintela, M. A.; Ishitobi, M.; Kunieda, H. *J. Colloid Interface Sci.* **2005**, *291*, 560–569.
- (69) Duval, M.; Waton, G.; Schosseler, F. *Langmuir* **2005**, *21*, 4904–4911.
- (70) Buhler, E.; Oelschlaeger, C.; Waton, G.; Candau, S. J. *J. Phys. Chem. B* **2004**, *108*, 11236–11243.
- (71) Buhler, E.; Munch, J. P.; Candau, S. J. *J. Phys. II* **1995**, *5*, 765–787.
- (72) Imanishi, K.; Einaga, Y. *J. Phys. Chem. B* **2005**, *109*, 7574–7581.
- (73) Brown, W.; Rymdiin, R. *J. Phys. Chem.* **1987**, *91*, 3565–3571.
- (74) Oelschlaeger, C.; Waton, G.; Buhler, E.; Candau, S. J.; Cates, M. E. *Langmuir* **2002**, *18*, 3076–3085.
- (75) Kato, T.; Nozu, D. *J. Mol. Liq.* **2001**, *90*, 167–174.
- (76) Semenov, A. N. *Phys. A* **1990**, *166*, 263–287.
- (77) Blanco, M. C.; Leisner, D.; Vazquez, C.; Lopez-Quintela, M. A. *Langmuir* **2000**, *16*, 8585–8594.